



CrossMark
click for updates

Cite this: *RSC Adv.*, 2015, 5, 42762

Template-free synthesis of nanoporous gadolinium phosphonate as a magnetic resonance imaging (MRI) agent†

Malay Pramanik,^a Fa-Kuen Shieh,^b Saad M. Alshehri,^c Zeid Abdullah Allothman,^c Kevin C.-W. Wu^{*de} and Yusuke Yamauchi^{*ac}

A new series of organic–inorganic hybrid porous gadolinium phosphonate (GdP) materials have been synthesized using benzene-1,3,5-triphosphonic acid as a phosphonic acid linker through a simple hydrothermal technique. The particle size and morphology are well controlled through the selection of suitable reaction conditions. The obtained materials exhibit very high specific surface area and crystalline pore walls with a triclinic structure having unit cell parameters $a = 7.76$ (3) Å; $b = 8.60$ (6) Å; $c = 14.09$ (7) Å; $\alpha = 100.08$ (4)°; $\beta = 84.23$ (6)°; $\gamma = 116.29$ (6)°. The obtained GdP materials are further used as a magnetic resonance imaging (MRI) contrast agent with r_1 and r_2 values of 2.6 and 4.7 s⁻¹ mM⁻¹, respectively.

Received 1st February 2015
Accepted 28th April 2015

DOI: 10.1039/c5ra02004b

www.rsc.org/advances

Introduction

Crystalline metal–organic solids with permanent porosity have a great scientific utility from last two decades because of their various applications in chemical and biological research.¹ Nanopores are sustained owing to the stable structure and strong coordinative interaction between metal ions and organic ligands.² Recently, metal–organic frameworks (MOFs) (or porous coordination polymers, PCP) have been extensively studied. The advantage of robust coordination bonds of MOFs has offered various kinds of MOFs with different organic linkers, thus providing well-defined crystal structure and porosity.^{3,4}

On one hand, phosphonate linkers are dianionic in nature and exhibit very strong interaction towards metal ions, which usually result in the formation of more robust solid.⁵ In this case, the growth of the metal–organic network is very rapid, and the solid products are immediately precipitated. However, the final products usually exhibit less ordered crystalline structure.⁶ Besides, in general, such a rapid precipitation

of materials leads to non-uniform porous structure.² On the other hand, the phosphonate linker with a pyramidal geometry has three adjacent oxygen atoms with phosphorus, thus it can force the metal ions to assemble in the liner fashion (with less surface area).^{2,7} So far, the synthesis of porous crystalline phosphonate materials with uniform pore diameter and high surface area has been limited to the utilization of different structure directing agents (SDAs). However, the removal of SDAs while remaining the original porous structure of the materials is still a challenge.

Consequently, a template-free synthesis of porous phosphonate materials with both high surface area and well-ordered crystalline structure has been highly demanded. It has been found that many of previous phosphonate materials were prepared from linear mono- or di-organo phosphonic acid ligands, and in those cases the synthesized metal–organic structures are formed as layered structures.⁸ Although various strategies using non-liner and mixed phosphonate linkers have been utilized to prepare non-layered phosphonate materials,^{6a,9} the successful synthesis of non-layered crystalline phosphonate materials with high surface area is still limited.^{6a,10}

Among all metal-phosphonate materials, Gd(III) phosphonate (GdP) nanomaterials have attracted much attention owing to their potential application as a MRI contrast agent. In this study, we selected benzene-1,3,5-triphosphonic acid, a non-liner linker, to prepare GdP materials with high porosity as well as high crystallinity without using any SDA (Scheme 1). By further tuning the synthetic conditions, we also successfully control the nano-architectures of the synthesized nanoporous GdP materials for MRI application. Previously, a few nanoporous Gd carboxylate nanomaterials and Gd-based hybrid nanoparticles have been used as a potential MRI contrast agent.¹¹ To the best of our best knowledge, however, this is the

^aInternational Center for Materials Nanoarchitectonics (MANA), National Institute for Materials Science (NIMS), 1-1 Namiki, Tsukuba, Ibaraki 305-0044, Japan. E-mail: Yamauchi.Yusuke@nims.go.jp

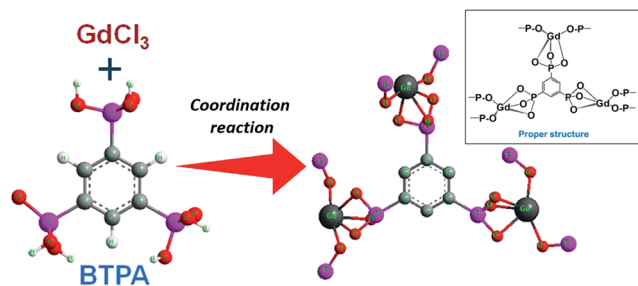
^bDepartment of Chemistry, National Central University, 300 Jhong-Da Road, Chung-Li 32001, Taiwan

^cChemistry Department, College of Science, King Saud University, Riyadh 11451, Saudi Arabia

^dDepartment of Chemical Engineering National Taiwan University, No. 1, Sec. 4, Roosevelt Road, Taipei 10617, Taiwan. E-mail: kevinwu@ntu.edu.tw

^eDivision of Medical Engineering Research, National Health Research Institutes, 35 Keyan Road, Zhunan, Miaoli County 350, Taiwan

† Electronic supplementary information (ESI) available. See DOI: 10.1039/c5ra02004b



Scheme 1 Synthetic pathway of formation of GdP materials.

first report of nanoporous GdP material used as a MRI contrast agent.

Experimental section

Materials

Commercially available 1,3,5-tribromobenzene, 1,3-diisopropylbenzene, triethyl phosphite (98%) and nickel(II) bromide and gadolinium(III) chloride hexahydrate (96%) were purchased from Sigma Aldrich.

Synthesis of BTPA

10 mmol (3.15 g) of 1,3,5-tribromobenzene was dissolved into 30 ml of 1,3-diisopropylbenzene by heating at 150 °C under inert atmosphere. Then the reaction mixture was cooled to room temperature and anhydrous nickel(II) bromide (500 mg) was added slowly to the reaction mixture under vigorous stirring under inert atmosphere. The reaction mixture was heated gradually to 180 °C and triethyl phosphite (7.5 ml) was added dropwise during 5–6 h. The heating was continued for next 6 h at the same temperature under inert atmosphere. Then the volatile components with 1,3-diisopropylbenzene were distilled off, and a dark viscous residue was collected. The compound hexaethyl-1,3,5-benzenetriphosphonate was purified over a column of silica gel eluted with CHCl_3 [CHCl_3 : MeOH = 10 : 1 (v/v)]. The colorless hexaethyl-1,3,5-benzenetriphosphonate was obtained by the solvent evaporation. The yield is 1.95 g (around 40%). 1.5 g of the product ester was hydrolyzed by 15 ml water in the presence of 10 ml concentrated HCl for 48 h. The hydrolyzed solution was evaporated to dryness and the residue was dissolved into 15 ml distilled water and decolorized by activated charcoal, then the filtrate was evaporate under reduced pressure to get a white solid, BTPA. The yield was 0.90 g (around 92%). The compound has been characterized by ^1H , ^{13}C , and ^{31}P NMR (Fig. S1†).

Synthesis of GdP materials

Four types of GdP materials are prepared by using different bases in the presence/absence of promoter (as listed in Table 1). In a typical synthetic condition, 0.33 mmol (0.106 g) of benzene-1,3,5-triphosphonic acid (BTPA) was dissolved into 5 ml of double distilled water and the pH of the solution was increased by 4.5 by NaOH, $(\text{Me})_4\text{NOH}$ or NH_4OH . In another closed vessel,

Table 1 Synthesis conditions for gadolinium(III) phosphonate materials (GdP)

Entry	Sample name	Base to maintain pH	Promoter
1	GdP-H	NaOH (12.5 wt%)	—
2	GdP-T	$(\text{Me})_4\text{NOH}$ (12.5 wt%)	—
3	GdP-A	NH_4OH (12.5 wt%)	—
4	GdP-AC	NH_4OH (12.5 wt%)	$^a\text{HClO}_4$ (0.25 ml)

^a HClO_4 solution is also used along with NH_4OH solution.

1 mmol (0.372 g) of gadolinium(III) chloride hexahydrate was dissolved in 10 ml double distilled water. Then, the synthetic solution was prepared by adding the mother BTPA solution (pH ~ 4.5) to the aqueous solution of gadolinium chloride. The pH of the final gel was maintained at 5 by the same base. The mixed solution was stirred for overnight and finally transferred to a Teflon-lined pressure vessel and kept at 180 °C for 36 hours. After that, the pressure vessel was cooled to room temperature very slowly (5 °C h^{-1}). The obtained material was collected by centrifugation and washing with ethanol for several times.

Characterizations

SEM images were taken with a Hitachi SU-8000 scanning microscope at an accelerating voltage of 15 kV. TEM observation was performed using a JEM-2010 TEM system that was operated at 200 kV. Wide-angle powder X-ray diffraction (XRD) patterns were obtained with a Rigaku RINT 2500X diffractometer using monochromated Cu $K\alpha$ radiation (40 kV, 40 mA) at a scanning rate of 0.1° min^{-1} . Nitrogen adsorption–desorption analyses were performed using a Belsorp-mini II Sorption System at 77 K. Specific surface areas were calculated by the Multipoint BET method at a P/P_0 range of 0.05–0.3. Total pore volumes were calculated by the Density Functional Theory (DFT) method. TG-DTA-MS was measured using a Rigaku Thermo Mass Photo TG-DTA-PIMS 410/S. X-ray photo-electronic spectroscopy (XPS) spectra were recorded at room temperature by using a JPS-9010TR (JEOL) instrument (Mg $K\alpha$ X-ray source). All the binding energies were calibrated by referencing to C 1s (285.0 eV). FT-IR spectra were recorded using an FT-IR spectrometer (Spectrum One, PerkinElmer L1200361) at room temperature.

Results and discussion

The morphology of the obtained GdP materials is determined by scanning electron microscope (SEM), as shown in Fig. 1. For GdP-H, GdP-A, and GdP-T, non-uniform spherical particles are mostly observed and their particle sizes are all about 100 nm. For GdP-AC material, it is interesting to note that the material has a flower-like morphology with *ca.* 100–150 nm in particle size. Such flower morphology is generated by randomly assembling uniform flakes of 3–4 nm in width (Fig. 1d). The representative TEM images for GdP-H and GdP-AC are shown in Fig. 1e and f, respectively. A disordered nanoporous structure can be clearly seen in the GdP-H (Fig. 1e). In contrast, the TEM image of the GdP-AC sample (Fig. 1f) shows aggregation of

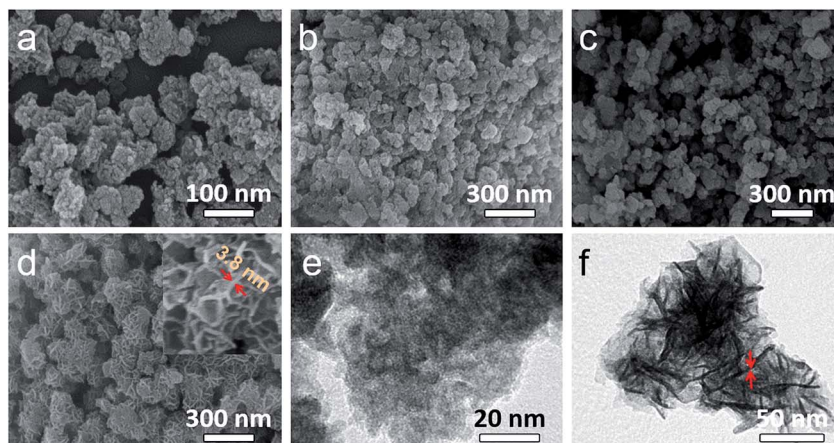


Fig. 1 SEM images of (a) GdP-H, (b) GdP-A, (c) GdP-T, and (d) GdP-AC, and TEM images of (e) GdP-H and (f) GdP-AC.

nanoflakes that is in a good agreement with the SEM image (Fig. 1d). In the cases of GdP-H, GdP-A and GdP-T, we suggest that there was no critical physical and chemical force for self-assembly. Therefore, to minimize the surface/volume ratio, the morphology of the materials became spheres. In contrast, GdP-AC synthesized with the presence of a promoter shows a totally different morphology, and the formation mechanism will be discussed below.

Wide-angle X-ray diffraction (XRD) patterns of the obtained GdP materials are shown in Fig. 2a. All the four materials have similar XRD patterns. Though the peak positions in the XRD pattern for each sample are the same, the crystallinity of GdP-AC is much higher over the other three samples. The crystal structure of the newly synthesized GdP materials does not match with any standard JCPDS literature profile. To solve this issue, the crystal structure of GdP-H material was determined by MAUD program (Fig. 2b),¹² and the diffraction pattern of the GdP-H material can be designated as a triclinic crystal phase with the unit cell parameters as follows: $a = 7.76$ (3); $b = 8.60$ (6); $c = 14.09$ (7); $\alpha = 100.08$ (4); $\beta = 84.23$ (6); $\gamma = 116.29$ (6).

Various oxyanions (e.g. chlorate, phosphate, and arsenate) have been served as a promoter to increase the crystallinity of various microporous materials, particularly zeolite-type

materials.¹³ With the increase of the polarization ability of oxyanions, the induction effect towards crystallization would increase gradually. Among all oxyanions, chlorate (ClO_4^-) has the highest polarization ability owing to the higher charge/radius value than other oxyanions.¹⁴ In our case, we used HClO_4 as the ClO_4^- source and serve as a promoter in the reaction medium. In the presence of ClO_4^- ions, the crystallinity of the final GdP material (i.e. GdP-AC) was increased hugely. Besides, the resulting morphology was also changed from spherical to flower-like.

To further characterize the framework structures, the FT-IR spectrum of GdP-H was measured between 4000 cm^{-1} to 400 cm^{-1} (Fig. S2†). The strong absorption peak at 556 cm^{-1} can be assigned to the Gd–O stretching vibration. The set of bands centered at 986 cm^{-1} and 1085 cm^{-1} can be assigned to the tetrahedral stretching vibration of $-\text{CPO}_3$ group. The peaks at 1402 cm^{-1} and 1520 cm^{-1} are the characteristic vibration bands of benzene ring in the GdP materials. The peak at 1635 cm^{-1} is probably due to the bending vibration of water molecules adsorbed in the surface of the material. One small peak around 2351 cm^{-1} is due to the CO_2 present in the environment of the experimental condition. The broad band centered at 3408 cm^{-1} is probably due to the defected P–OH group in the material and free water molecule attached to the surface of the porous

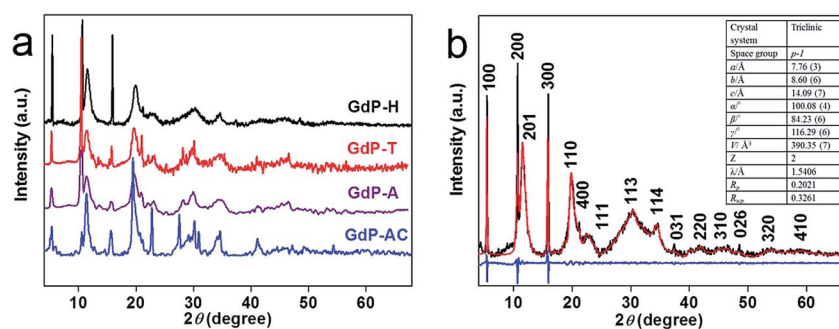


Fig. 2 (a) Wide-angle X-ray diffraction patterns of GdP-H, GdP-T, GdP-A and GdP-AC, respectively, and (b) experimental XRD pattern of GdP-H (black line), computed XRD pattern (red line), and the difference between the experimental and the computed XRD patterns (blue line). The crystal parameters of GdP, including lattice parameters and R factors, are also shown.

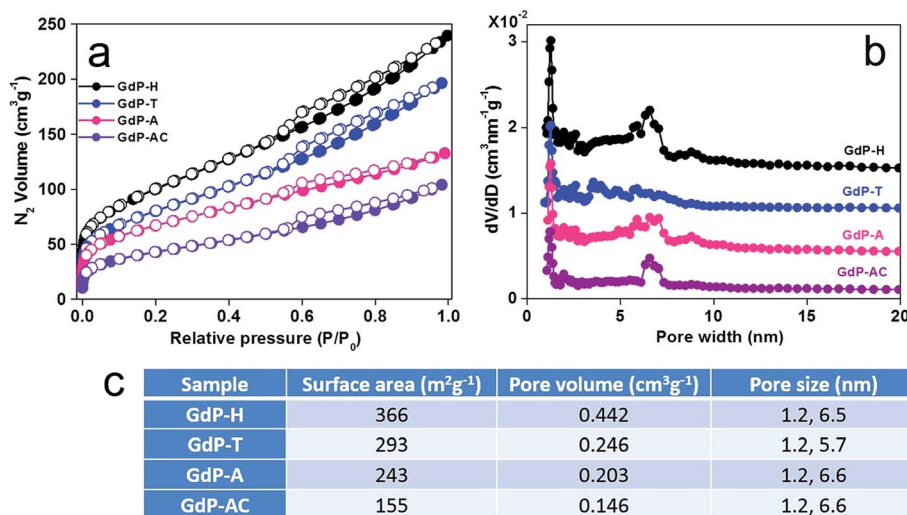


Fig. 3 N₂ adsorption (filled circles)–desorption (empty circles) isotherms of (a) GdP-H, GdP-T, GdP-A, and GdP-AC, (b) pore size distribution curves, and (c) summary of surface area, pore volume, and pore diameter of the GdP materials.

material. On the basis of the FT-IR analysis, we propose the presence of BTPA and Gd inside the porous framework of GdP-H.¹⁵

The architectural porosity of the synthesized GdP materials was determined by N₂ adsorption–desorption isotherms (Fig. 3a). The corresponding BET specific surface area, pore volume and pore diameter of the materials are listed in Fig. 3c. The adsorption–desorption isotherms of the materials show the typical type-II with small hysteresis loops. There is a pronounced stage of monolayer adsorption on the materials owing to the presence of appreciable amount of micropores in the materials. When the relative pressure (P/P_0) was over 0.01, multilayer adsorption took place and amount of adsorption increased gradually as the relative pressure increased, suggesting the presence of relevant amount of mesopores in the materials. Because of the presence of significant amount of mesopores in the materials at higher relative pressure ($P/P_0 > 0.5$), the capillary condensation and evaporation did not take place at same relative pressure, thereby observing the hysteresis loops.¹⁶ The corresponding pore size distribution curves were calculated by Density Functional Theory (DFT) (Fig. 3b). The GdP-H and GdP-AC samples exhibited the highest and lowest surface area (366 and 155 m² g⁻¹, respectively) among all the samples. The low surface area and pore volume of GdP-AC were due to the dense packing of the π -electron rich benzene rings.

X-ray photoelectron spectroscopy (XPS) is a powerful tool to determine not only the electronic structure but also the chemical composition and local structure of samples. From the XPS spectrum of GdP-H (Fig. 4a), we can confirm the presence of elements carbon, gadolinium, oxygen and phosphorus in the material. The EDX measurement of GdP-H and GdP-AC also proves the presence and homogeneous distribution of C, P, Gd and O throughout the specimens (Fig. S3 and S4†). The high-resolution XPS spectra of Gd 3d and Gd 4d state reveals that the two energy states split into doublets due to the

spin orbit coupling. The corresponding energy levels are Gd 3d_{3/2}, Gd 3d_{5/2}, Gd 4d_{3/2}, and Gd 4d_{5/2} with the peaks at 1220.60, 1188.12, 149.68, and 143.28 eV, respectively (Fig. 4b and c). The line shape and the peak positions are consistent with the previously reported gadolinium phosphate materials.¹⁷ The energy level of P 2p also splits into doublet (2p_{1/2} and 2p_{3/2} at 143.51 and 133.71 eV, respectively) (Fig. 4d). The high-resolution XPS spectrum for C 1s was also measured (Fig. 4e) and the peak is located at 285.02 eV. The elemental compositions (C : P : Gd) are estimated to be 2.09 : 1.00 : 1.01, which is very close to the elemental ratio of the calculated molecular formula of C₆P₃O₉Gd_{2.9}·*n*H₂O. Here the charge of one Gd³⁺ is full-filled by three ≡P–O[–] bonds. So, to maintain the proper charge-balance structure and co-ordination number of Gd (tetrahedral/octahedral) and P (tetrahedral), the macromolecular assembly is formed to produce the porous architecture (inset of Scheme 1).

The thermal stability of the synthesized porous GdP materials was investigated by TG-DTA analysis under the continuous flow of air with a heating rate of 5 °C min⁻¹. All the four samples show almost the same TG-DTA profiles. The TG plot of the GdP-H shows two distinct weight loss of the material (Fig. S5†). The first weight loss (16.6 wt%) up to 550 K is due to the removal of surface-adsorbed water molecules in the porous framework of the material. The second weight loss in the range 620 K to 1000 K is due to the burning of C–C and C–P bonds in the material. From the TG-DTA curve, it can be concluded that the synthesized materials have good thermal stability.

The free/un-coordinated phosphonic acid is the prime source of acidity of this type of materials. We investigated the acidic behavior of GdP-H material in water and PBS pH 7 buffer solution. In case of water, the solution become a little acidic (pH ~ 6) after treating with GdP-H material, while in case of PBS pH 7 buffer solution the pH of the solution do not change at all after treating with GdP-H material. From this result, we can predict that the GdP-H material has little free/un-coordinated

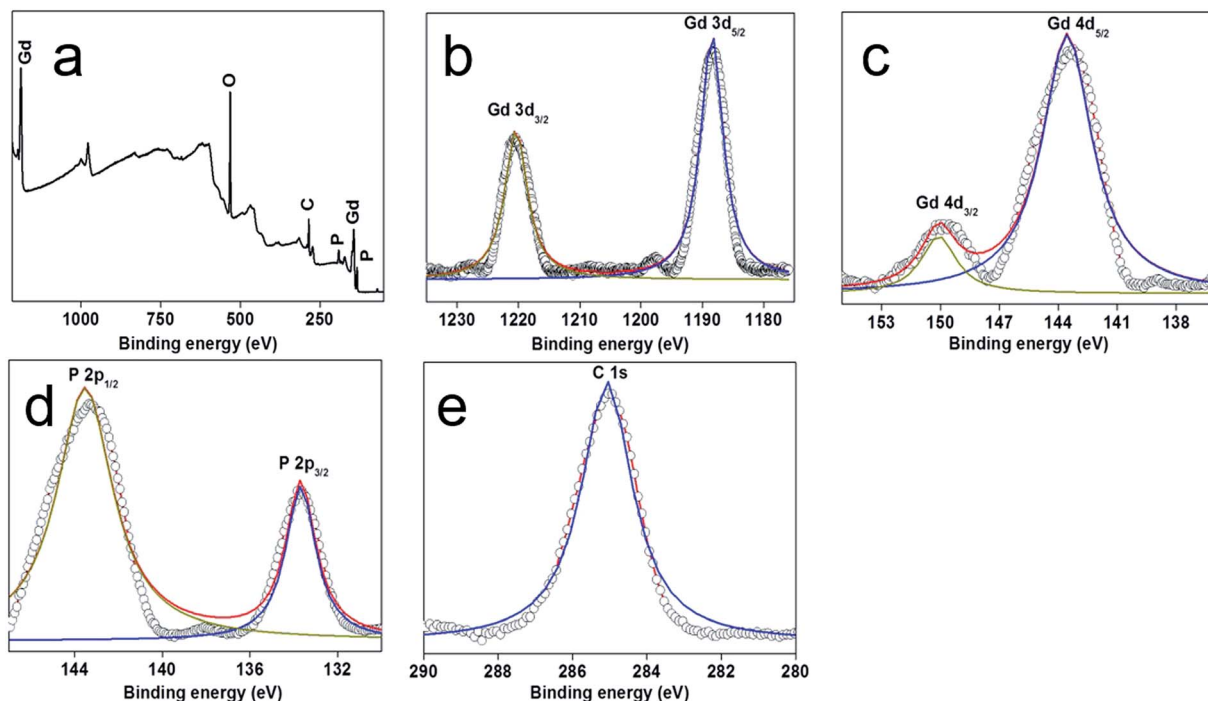


Fig. 4 XPS data of GdP-H (a) survey spectrum, (b) Gd 3d, (c) Gd 4d, (d) P 2p, and (e) C 1s.

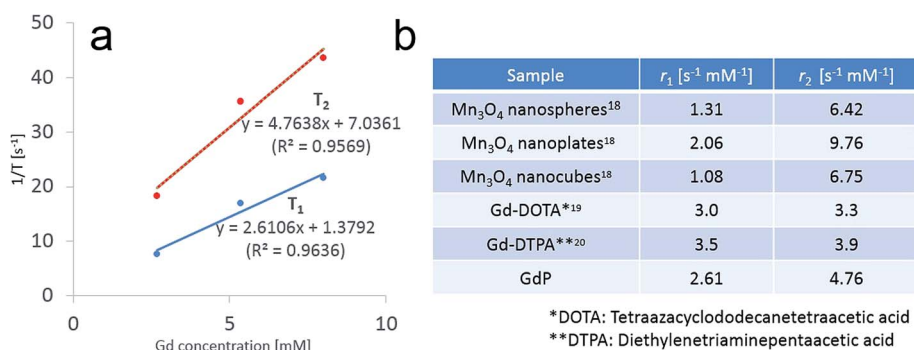


Fig. 5 (a) Relaxivity intensity plots of T_1 and T_2 signals in xanthan gum containing of GdP-H nanoparticles with various concentrations. (b) Comparison of the obtained r_1 and r_2 values with other materials.

phosphonic acids. The stability of the GdP-H material has also examined by water treatment for 24 hours. Even after water treatment, the wide angle XRD pattern and the surface area of the GdP-H material remain unchanged, indicating that the material does not dissociate in normal atmospheric condition (Fig. S6†).

The obtained GdP materials can be used as a magnetic resonance imaging (MRI) contrast agent. A gradient system mounted on the table of a 9.4 T magnet was used to generate images with high resolution.¹⁸ The GdP-H sample with various concentrations of Gd (2.7–8.0 mM) were mixed in 0.3% xanthan gum. The corresponding r_1 and r_2 values were calculated based on the inverse relaxation time ($1/T_1$) and ($1/T_2$) versus Gd concentrations in the gum.^{19,20} The r_1 and r_2 values were 2.6 $s^{-1} mM^{-1}$ and 4.7 $s^{-1} mM^{-1}$, respectively. The obtained r_1 and r_2 relaxivity are almost the same as those Gd³⁺-containing samples

reported previously.^{19,20} Here we have also compared our result with previously reported various Mn₃O₄ materials (Fig. 5b). And it has been found that our materials have good/comparable activity with the previously reported Mn₃O₄ materials.¹⁸ Although it has been reported that the Gd³⁺ locating near the surface of the samples would exhibit higher relaxivity, in this study the ease and reliable synthesis process could easily produce Gd³⁺-containing nanoparticles with diameter of about 100 nm, thereby creating more Gd³⁺ on the surface and thus showing great potential for efficient intracellular MRI contrast agents in the future. However, it has been well known that as a MRI contrast agent, surface coating is sometimes necessary for Gd-containing nanoparticles because of the high toxicity of Gd. Therefore, surface functionalization with polymers that exhibit high biocompatibility and cell-targeting ability will be the future work.

Conclusion

We have reported a simple and template-free hydrothermal method for the synthesis of crystalline, nanoporous GdP nanoparticles with different morphologies by using benzene-1,3,5-triphosphonic acid (BTPA) as organic scaffold. The GdP nanomaterials have very high surface area with triclinic crystal phase. Our newly developed GdP nanomaterials have been successfully used as a magnetic resonance imaging (MRI) contrast agent with r_1 and r_2 values of 2.6 and $4.7 \text{ s}^{-1} \text{ mM}^{-1}$, respectively. We believe that a very facile synthesis of Gd-containing nanomaterials, with large internal surface area and remarkable efficiency as a MRI contrast agent, would open new avenues for *in vivo* study in near future.

Acknowledgements

The authors acknowledge the financial support of this work by King Saud University through National Plan for Science and Technology grant (NPST ADV 2120-02).

References

- (a) J. A. Hurd, R. Vaidhyanathan, V. Thangadurai, C. I. Ratcliffe, I. L. Moudrakovski and G. K. H. Shimizu, *Nat. Chem.*, 2009, **1**, 705–710; (b) J. D. Rocca, D. Liu and W. Lin, *Acc. Chem. Res.*, 2011, **44**, 957–968; (c) Y. Yamauchi, *J. Ceram. Soc. Jpn.*, 2013, **121**, 831–840; (d) J. Ye and C. Liu, *Chem. Commun.*, 2011, **47**, 2167–2169; (e) A. R. Millward and O. M. Yaghi, *J. Am. Chem. Soc.*, 2005, **127**, 17998–17999; (f) J. J. Perry, J. A. Perman and M. J. Zaworotko, *Chem. Soc. Rev.*, 2009, **38**, 1400–1417; (g) Y. Yamauchi, N. Suzuki, P. Gupta, K. Sato, N. Fukata, M. Murakami, T. Shimizu, S. Inoue and T. Kimura, *Sci. Technol. Adv. Mater.*, 2009, **10**, 1–9.
- J. M. Taylor, A. H. Mahmoudkhani and G. K. H. Shimizu, *Angew. Chem., Int. Ed.*, 2007, **46**, 795–798.
- (a) M. Eddaoudi, D. B. Moler, H. L. Li, B. L. Chen, T. M. Reineke, M. O’Keeffe and O. M. Yaghi, *Acc. Chem. Res.*, 2001, **34**, 319–330; (b) N. Stock and S. Biswas, *Chem. Rev.*, 2012, **112**, 933–969; (c) O. M. Yaghi, M. O’Keeffe, N. W. Ockwig, H. K. Chae, M. Eddaoudi and J. Kim, *Nature*, 2003, **423**, 705–714.
- (a) X. Zhao, B. Xiao, A. J. Fletcher, K. M. Thomas, D. Bradshaw and M. J. Rosseinsky, *Science*, 2004, **306**, 1012–1015; (b) R. Matsuda, R. Kitaura, S. Kitagawa, Y. Kubota, R. V. Belosludov, T. C. Kobayashi, H. Sakamoto, T. Chiba, M. Takata, Y. Kawazoe and Y. Mita, *Nature*, 2005, **436**, 238–241; (c) L. Pan, M. B. Sander, X. Huang, J. Li, M. Smith, E. Bittner, B. Bockrath and J. K. Johnson, *J. Am. Chem. Soc.*, 2004, **126**, 1308–1309.
- (a) G. Alberti, F. Marmottini, S. M. Mascarpis and R. Vivani, *Angew. Chem., Int. Ed.*, 1994, **33**, 1594–1597; (b) M. D. M. Gpmez-Alcántara, A. Cabeza, L. Moreno-Real, M. A. G. Aranda and A. Clearfield, *Microporous Mesoporous Mater.*, 2006, **88**, 293–303.
- (a) M. Vasylyev and R. Neumann, *Chem. Mater.*, 2006, **18**, 2781–2783; (b) N. A. Khan, I. J. Kang, H. Y. Seok and S. H. Jung, *Chem. Eng. J.*, 2011, **166**, 1152–1157.
- (a) J. Liang and G. K. H. Shimizu, *Inorg. Chem.*, 2007, **46**, 10449–10451; (b) C. Serre, J. A. Groves, P. Lightfoot, A. M. Z. Slawin, P. A. Wright, N. Stock, T. Bein, M. Haouas, F. Taulelle and G. Férey, *Chem. Mater.*, 2006, **18**, 1451–1457.
- (a) G. Cao, H. G. Hong and T. E. Mallouk, *Acc. Chem. Res.*, 1992, **25**, 420–427; (b) P. Barber, H. Houghton, S. Balasubramanian, Y. K. Anguchamy, H. J. Ploehn and H. C. Z. Loye, *Chem. Mater.*, 2009, **21**, 1303–1310.
- (a) G. Alherti, U. Costantino, F. Marmottini, R. Vivani and P. Zappelli, *Angew. Chem., Int. Ed. Engl.*, 1993, **32**, 1357–1359; (b) M. V. Vasylyev, E. J. Wachtel, R. P. Biro and R. Neumann, *Chem.–Eur. J.*, 2006, **12**, 3507–3514.
- G. Guerrero, P. H. Mutin and A. Vioux, *Chem. Mater.*, 2000, **12**, 1268–1272.
- (a) W. J. Rieter, K. M. L. Taylor, H. An, W. Lin and W. Lin, *J. Am. Chem. Soc.*, 2006, **128**, 9024–9025; (b) H. Hifumi, S. Yamaoka, A. Tanimoto, D. Citterio and K. Suzuki, *J. Am. Chem. Soc.*, 2006, **128**, 15090–15091.
- L. Lutterotti, MAUD version 1.85, 2002, <http://www.ing.unitn.it/~maud/>.
- R. Kumar, A. Bhaumik, R. K. Ahedi and S. Ganapathy, *Nature*, 1996, **381**, 298–300.
- R. Kumar, P. Mukherjee, R. K. Pandey, P. Rajmohan and A. Bhaumik, *Microporous Mesoporous Mater.*, 1998, **22**, 23–31.
- M. Pramanik and A. Bhaumik, *Chem.–Eur. J.*, 2013, **19**, 8507–8514.
- (a) M. Kruk and M. Jaroniec, *Chem. Mater.*, 2001, **13**, 3169–3183; (b) D. Zhao, D. Yuan, D. Sun and H. C. Zhou, *J. Am. Chem. Soc.*, 2009, **131**, 9186–9188.
- A. A. Guay-Begin, P. Chevallier, L. Faucher, S. Turgeon and M. A. Fortin, *Langmuir*, 2012, **28**, 774–782.
- C. C. Huang, N. H. Khu and C. S. Yeh, *Biomaterials*, 2010, **31**, 4073–4078.
- C. H. Su, H. S. Sheu, C. Y. Lin, C. C. Huang, Y. W. Lo, Y. C. Pu, J. C. Weng, D. B. Shieh, J. H. Chen and C. S. Yeh, *J. Am. Chem. Soc.*, 2007, **129**, 2139–2146.
- I. F. Li, C. H. Su, H. S. Sheu, H. C. Chiu, Y. W. Lo, W. T. Lin, J. H. Chen and C. S. Yeh, *Adv. Funct. Mater.*, 2008, **18**, 766–776.